Int. J. Electrochem. Sci., 11 **(2016)** 5766 – 5780, doi: 10.20964/2016.07.41

International Journal of
ELECTROCHEMICAL
SCIENCE
www.electrochemsci.org

The perovskite $Ba_{0.5}Sr_{0.5}Co_{0.2}Fe_{0.8}O_3$-MWCNT modified glassy carbon electrode – Its Characterization and Capacity in Oxygen Reduction Reaction

F. Yusoff[1,2], *N. Mohamed*[1], *A. Azizan*[3], *S. Ab Ghani*[1*]

[1]Pusat Pengajian Sains Kimia, Universiti Sains Malaysia, 11800, Pulau Pinang, Malaysia
[2]Pusat Pengajian Sains Marin dan Sekitaran, Universiti Malaysia Terengganu, 21030, Kuala Terengganu, Terengganu, Malaysia
[3]Pusat Pengajian Sumber Bahan dan Mineral, Kampus Kejuruteraan, Universiti Sains Malaysia, 14300, Pulau Pinang, Malaysia
[*]E-mail: sag@usm.my

Received: 3 December 2015 / *Accepted:* 21 March 2016 / *Published:* 4 June 2016

The modified glassy carbon electrodes (GCE) are prepared by chemical deposition of $Ba_{0.5}Sr_{0.5}Co_{0.2}Fe_{0.8}O_3$ (BSCF), multi-walled carbon nanotube (MWCNT) and BSCF-MWCNT. The GCE, BSCF/GCE, MWCNT/GCE and BSCF-MWCNT/GCE electrodes are characterised by scanning electron microscopy (SEM), atomic force microscopy (AFM), cyclic voltammetry (CV) and electrochemical impedance spectroscopy (EIS). The surface morphology studies show that MWCNT is homogenously dispersed on the surface of BSCF. The N_2 isotherm study indicates that surface area is improved by three fold than the BSCF alone. The EIS and CV show that the presence of MWCNT is significant in enhancing the electronic conductivity as well as kinetics. The reduction behaviours of these electrodes in 0.1 M KOH are compared using chroroamperometry, CV and hydrodynamic voltammetry. The BSCF-MWCNT/GCE shows a pronounced electrocatalytic activity towards oxygen reduction.

Keywords: $Ba_{0.5}Sr_{0.5}Co_{0.8}Fe_{0.2}O_3$ (BSCF), multiwall carbon nanotube (MWCNT), oxygen reduction reaction (ORR)

1. INTRODUCTION

The oxygen reduction reaction (ORR) is a fundamental reaction associated to various disciplines such as energy conversion (alkaline fuel cells [1], metal air batteries [2]), hydrogen peroxide production [3], as an auxiliary reaction of oxidative electro-syntheses [4] and galvanic sensor

for dissolved oxygen [5]. ORR can occurs either by direct four-electron process or two-electron pathway giving the following reactions:

Four-electron process

$$O_2 + 4H^+ + 4e^- \rightarrow 2H_2O \quad (1)$$

Two electron process

$$O_2 + 2H^+ + 2e^- \rightarrow H_2O_2 \quad (2)$$

$$H_2O_2 + 2H^+ + 2e^- \rightarrow 2H_2O \quad (3)$$

To date, it is still a challenge to find the exact pathway/mechanism of the ORR because of its complex kinetics. Many researchers are doing their best to find suitable electrocatalysts that could support the desired four-electron reduction process leading to efficient energy conversion [6-8]. The mechanism of the ORR is known to be highly sensitive to the type of electrode materials, their surface structures, surface modifiers and the nature of the electrolytic solution. Tremendous efforts have been devoted to develop the electrode that can facilitate the electron transfer rate in slow electrochemical reactions. The current research involves the utilization of modified electrodes which have been constructed by introducing the catalysts at the electrode surface [9-10]. Hence, a wide variety of compounds such as manganese oxide [11], copper [12], ruthenium–iron cluster [13], metal phthalocyanine [14], metal macrocyclic complexes [15], and perovskite oxide have been proposed as electrocatalysts for the reduction of oxygen.

Many researchers have studied the electro-reduction properties of oxygen on perovskite structured oxides [16-17] after it is introduced by Meadowcroft [18]. Among the evaluated perovskite type oxides, ABO_3 perovskite (A = La, Ca, or Sr, and B = Co, Fe, or Mn), the cobaltites (B=Co) were demonstrated to be catalytically active but chemically unstable [19] contrary to the ferrites (B = Fe) which were very stable but hardly active [20]. The perovskites show outstanding cathodic oxygen reduction characteristic in alkaline media when mixed with high surface area elements/compounds such as carbons. The activity of these oxide electrocatalysts are correspond to the capacity of the B cations to accept distinctive valency states during the formation of redox couples at the potential of oxygen reduction [21].

One of these perovskite, $Ba_{0.5}Sr_{0.5}Co_{0.2}Fe_{0.8}O_3$ (BSCF) which has been reported to be an effective cathode materials for fuel cell. These materials have been extensively investigated as oxygen permeation membrane material for oxygen generation [22-23]. However, due to the lower electronic conductivity of the BSCF, the ORR reactions at these materials produce inefficient energy [24]. If this is improved, it could promote the oxygen surface exchange at the cathode [25]. The catalytic activity of the BSCF modified electrode can be enhanced by increasing its surface area.

Electrodes modified with nanoparticle materials have their properties significantly enhanced owing to the high surface area-to-volume ratio, superior electronic properties and higher chemical stability. [26-28]. Multiwall carbon nanotubes (MWCNT) represent one of the best examples of nanomaterials derived from bottom-up chemical synthesis approaches. After being discovered by Iijima [29], the potential application of carbon nanotube (CNT) has been extensively studied [30-32].

These materials exhibit excellent potential in the fields of catalysis [33], chromatography [34], nanoprobes [35] and biosensing [36].

In this study, the BSCF, MWCNT and BSCF/MWCNT are prepared, characterized and investigated for its performance in application to ORR. The electrochemical behavior, efficiency and stability of the electrodes in the electrocatalysis of oxygen reduction by cyclic voltammetry and rotating-disk electrode (RDE) voltammetry techniques are discussed. The application of modified BSCF-MWCNT in ORR has not yet been reported elsewhere.

2. EXPERIMENTAL

2.1. Materials and equipment

The MWCNT (8–15 nm OD, 3–5 nm ID, 50 μm length, purity >95%) was obtained from Chengdu Organic Chemicals Co. Ltd., Chinese Academy of Sciences, China. Ethylene diamine tetraacetic acid (EDTA), potassium ferrocyanide (99.0 %), potassium chloride (99.0 %), anhydrous citric acid, potassium hydroxide (KOH), sodium percholarate ($NaClO_4$) ,barium (II) nitrate, strontium (II) nitrate, cobalt (II) nitrate, and iron (III) nitrate, were purchased from Sigma Aldrich, USA and were used as received. Purified H_2O_2 (30%) and ammonia solution each have been purchased from Merck, Germany and Systerm Chemicals, Australia. Millipore Direct – Q3 (18.2 MΩcm) of Millipore, USA were used to prepare aqueous solutions

The morphological studies were carried out by using field emission scanning electron microscopy (FESEM) LEO SUPRA 55VD ultra-high resolution of Zeiss, Germany. Atomic Force Microscopy (BRUKER, Germany) and Nanoscope Analysis software is used to examine surface topology of the electrodes. Electrochemical measurements were performed with a standard single compartment three electrode cell having a Pt counter electrode, a glassy carbon working electrode, and Ag/AgCl (3.0 M KCl) reference electrode, employing a Potentiostat/Galvanostat EG&G Model 273A (Princeton Applied Research, USA) with Power Suite program. AC impedance were measured using an EG&G Frequency Response Detector 100 completed with ZSimpWin 3.22 software of Princeton Applied Research, USA over a frequency range of 100 kHz to 100 mHz and AC voltage amplitude 5 mV.

2.2. Synthesis of BSCF and MWCNT powder

BSCF precursors powders was prepared by sol gel method [37] using nitrate salts of barium (II), strontium (II), cobalt (II) and iron (III) as starting materials. The powders obtained is then calcined at 1000˚C and kept in desiccator. The MWCNT was purified by acid-treatment method using 6 M of HCl. Then, 50 mg of purified MWCNT was bath sonicated in 40 mL mixture of H_2SO_4/HNO_3 (v:v = 3:1) for 7 h at 40 ˚C. It was then filtered and rinsed with distilled water, until the pH of the filtrate was neutral. The final solid was dried at 120°C in vacuum to a constant weight.

2.3. Electrode preparation

Before any modification, a glassy carbon electrode (GCE) of Metrohm (3 mm diameter) must be polished with 0.2 μm of alumina slurry prior until smooth, mirror-like surface was obtained. The GCE was individually cleaned in ultrasonic bath for 5 min using ethanol and distilled water. 1 mg of each ball-milled powder of BSCF is mixed with 1.0 mL N, N- dimethylformamide (DMF) to be sonicated at 40°C for 30 minutes. A 200 μL of the mixture is slowly dripped onto the glassy carbon (GC) electrode and then dried. A stock solution of 1 mg mL^{-1} MWCNT-DMF is prepared by dispersing 1 mg of MWCNT in 1 mL DMF. A 50 μL of MWCNT-DMF solution is then casted on top of BSCF before drying at room temperature. The resulting electrodes were BSCF/GCE, MWCNT/GCE and BSCF-MWCNT/GCE.

2.4. Electrochemical measurements

The electrode performance of the bare GCE, BSCF/GCE, MWCNT/GCE and BSCF-MWCNT/GCE were studied by cyclic voltammogram in the applied potential region of -0.2 to 0.8 V vs Ag/AgCl in ferricyanide/ferrocyanide solution at various scan rates. The EIS measurement was immediately performed after cyclic voltammetry. A sinusoidal signal with amplitude of 5 mV rms was applied. The modulus and phase were plotted over a frequency range of 100 kHz to 100 mHz. Oxygen reduction behavior of modified GCE were investigated using rotating disk electrode in 15 mL 0.1 M KOH earlier deaerated by purging N_2 and O_2 gas for 10 min. The experiment were scanned several times in the potential range of -1.1 to 0.2 V to obtain constant responses.

3. RESULT AND DISCUSSION

3.1. Surface morphology of modified electrode

It is clearly seen in the SEM photomicrograph that the fibrous network of MWCNT is homogenously dispersed throughout the surface of BSCF (Figure 1). The composite material (BSCF-MWCNT) is examined further by using AFM. Figure 2A shows agglomerated BSCF particles with obvious difference in depth. With the addition of MWCNT (Figure 2B), the presence of smaller particle is clearly reflected in the 3D image indicating the successful formation of the composite. The image reveals that the MWCNT distribution on BCSF matrix is homogenous throughout the matrix which is supported by SEM data.

The uniform distribution of MWCNT contributes to higher surface area of the composite. It leads to the increase in electrochemically active surface area available for reaction. Coverage of the MWCNT during the deposition process. It also indicates that the particles are mono-disperse. The AFM images documented cells with less regular structure after coating with MWCNT, compared with uncoated BSCF. The root mean square (RMS) roughness of surface is about 51.2 and 7.7 nm for BSCF

and BSCF-MWCNT respectively (based on calculating the deviations of surface height data by AFM software). Decrease in surface roughness is direct evidence of the high-density

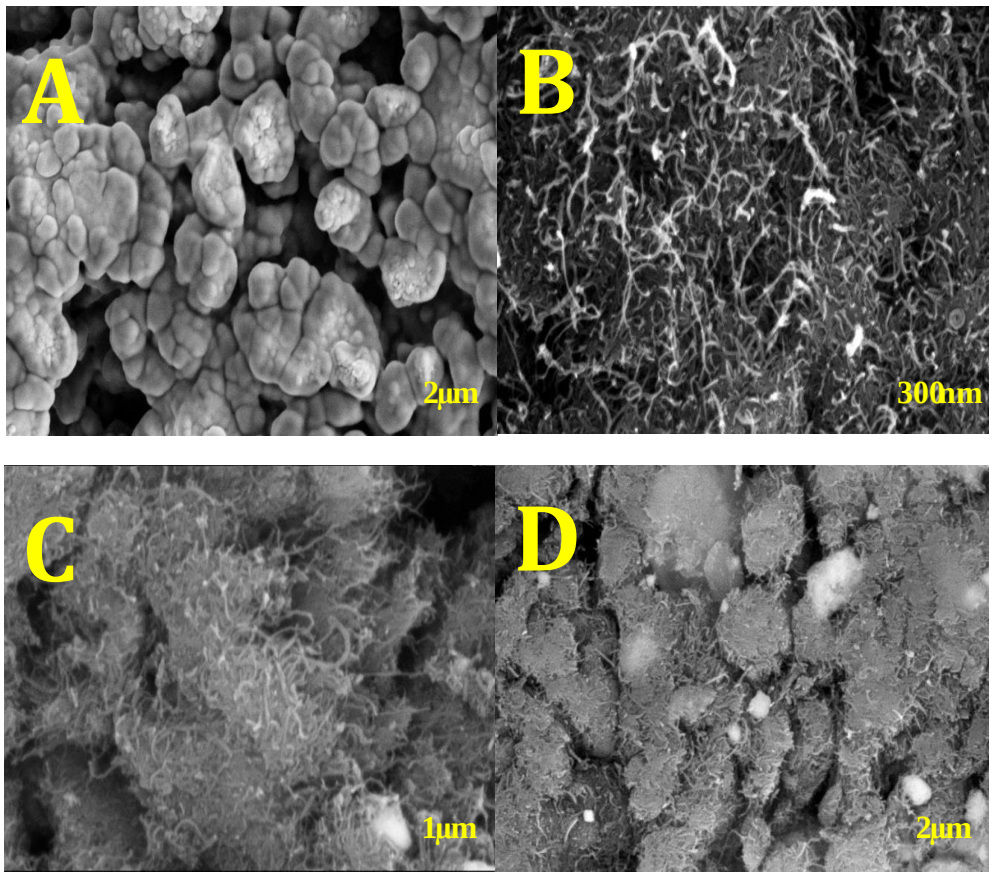

Figure 1. SEM images of (A) BSCF, (B) MWCNT (C) BSCF-MWCNT at 20X magnification (D) BSCF-MWCNT at 10X magnification.

The surface area of the electrodes is further studied by N_2 adsorption-desorption isotherms Information on surface area is summarized in Table 1. The specific surface areas (S_{BET}) calculated from BET equation have increase significantly with the presence of MWCNT in the composites. This is mainly due to the increase of the micropores surface area. However, the Langmuir surface areas show a considerably different result since only the area covered by one layer of gas is calculated. BSCF-MWCNT composites have a greater tendency of adsorption because the strength of a porous material depends directly on the total pore volume [38].

Table 1. The pore structure parameter and surface area

Electrodes	S_{BET} (m^2g^{-1})	Pore size, D_w (nm)	Pore volume (cm^3g^{-1})	Langmuir surface area (m^2g^{-1})
BSCF	14.4	4.5	0.016	42.6
MWCNT	109.5	2.5	0.76	224.7
BSCF-MWCNT	58.8	2.7	4.04	95.86

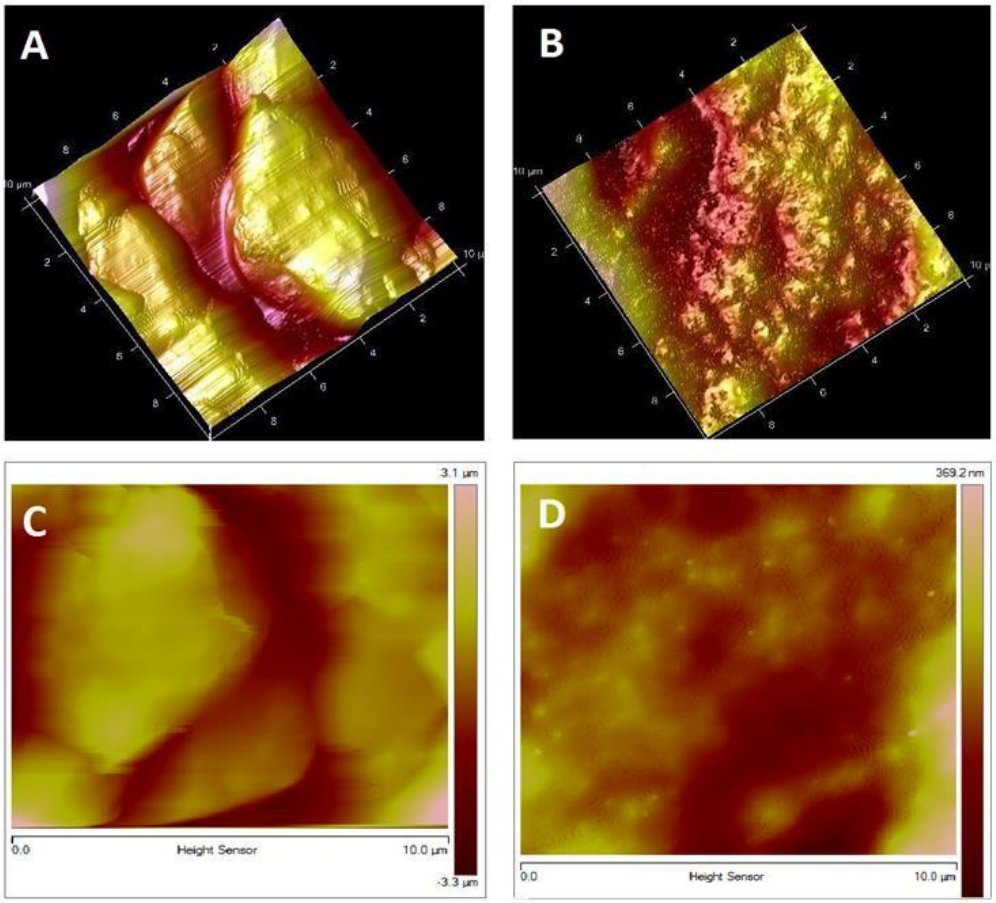

Figure 2. AFM images of BSCF and BSCF coated with MWCNT; (A) 3D view of BSCF (B) 3D view of BSCF-MWCNT (C) 2D view of BSCF and (D) 2D view of BSCF-MWCNT.

3.2. Cyclic voltammetry

The CVs of bare GCE, BSCF/GCE, MWCNT/GCE and BSCF-MWCNT/GCE in the applied potential range of -0.2 V to 0.8 V at the scan rate of 50 mVs^{-1} electrode have been investigated. From Figure 3(a), all electrodes show a well-defined redox peak with very high electrochemical activity. It is obvious that the larger surface area of BSCF-MWCNT/GCE has improved the kinetic of electron transfer by leap and bound as compared to the BSCF/GCE and bare GCE. It is also noticeable that the significance of BSCF in catalytic effect on the bare GCE. After continuous scanning for 50 cycles (data not shown), 95% of the initial current response was remained, which represent the modified electrode stability. The redox peak currents are proportional to the square root of the scan rate, $\nu^{1/2}$ (inset in Figure 3b) showing the diffusion controlled electron-transfer process. The electron transfer rate constant (k_s) and charge transfer coefficient (α) can be calculated from the variation of ΔE_p *vs*. log scan rate (Figure 4). Using the Eq (4):

$$E_p = K - 2.3030\ (RT/\alpha nF)\ \log(\nu) \qquad (4)$$

Considering one electron is transferred for the electrodes, α value can be obtained. By introducing α value in Eq. 5, an apparent surface electron transfer rate constant, k_s can be determined.

$$E_p = E^0 - \frac{RT}{\alpha nF}\ln\frac{RTk_s}{\alpha nF} + \frac{RT}{\alpha nF}\ln v \qquad (5)$$

Where E˚ is formal standard potential, n the number of the electrons transferred involved, while F, R and T have their usual meaning. From Table 2, α and k_s values for BSCF-MWCNT/GCE enhanced to that of BSCF/GCE. However MWCNT/GCE gives the highest electron transfer rate constant. The large value of k_s indicates higher ability of MWCNT to assist transfer of electron between electrode surface and the electrolyte. This is due to the MWCNT surfaces that consist of large amount of defects and also the superior nanostructure of MWCNT which can act as molecular wires in enhancing the impulsive electron transfer at the electrode. This suggest that MWCNT is a suitable modifier to assist the electron transfer of the modified BSCF-MWCNT/GCE electrode.

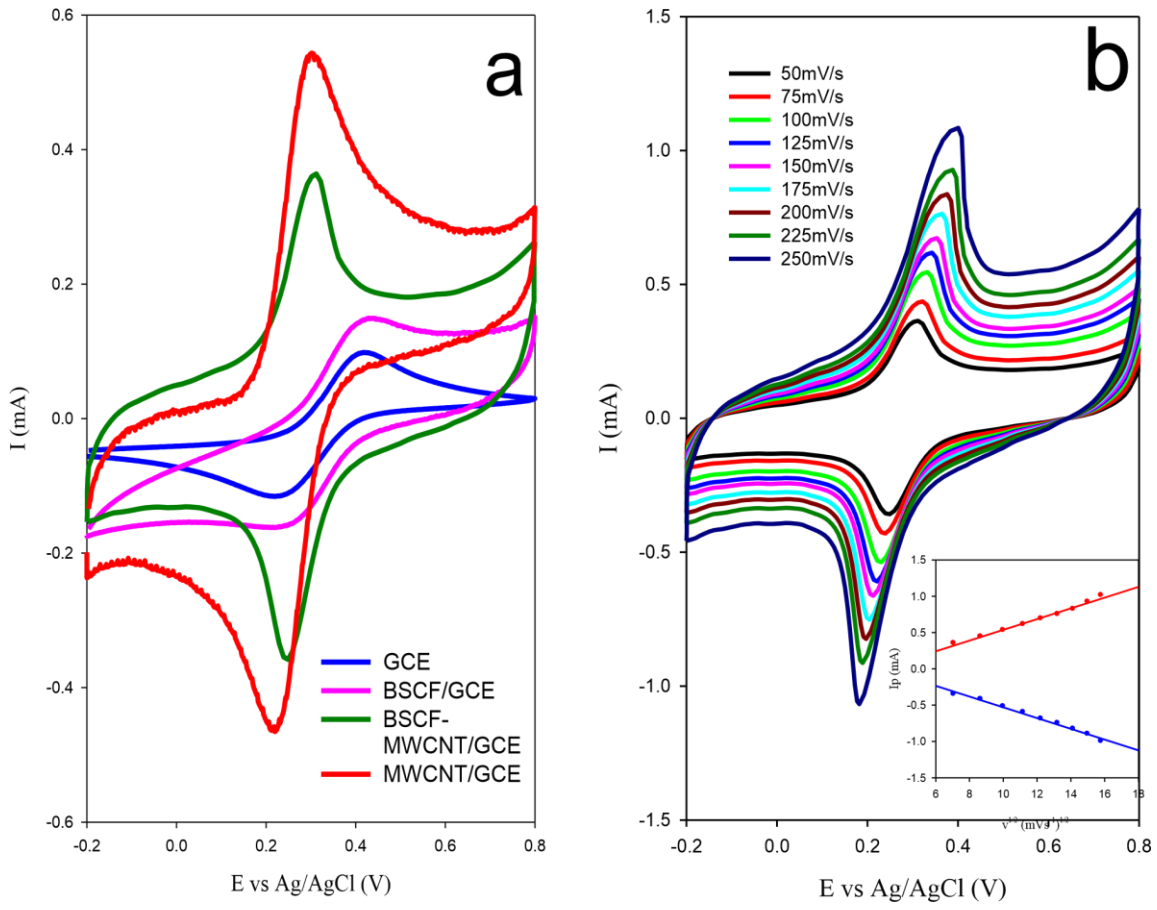

Figure 3. (a) Cyclic voltammograms of GCE, BSCF/GCE, MWCNT/GCE and BSCFMWCNT/GCE in 5 mM $[Fe(CN)_6]^{4-/3-}$ and 0.1 M KCl (b) CV scans of BSCF-MWCNT/GCE recorded at different scan rates (Inset: linear relationship in peak current vs the square root of the scan rate).

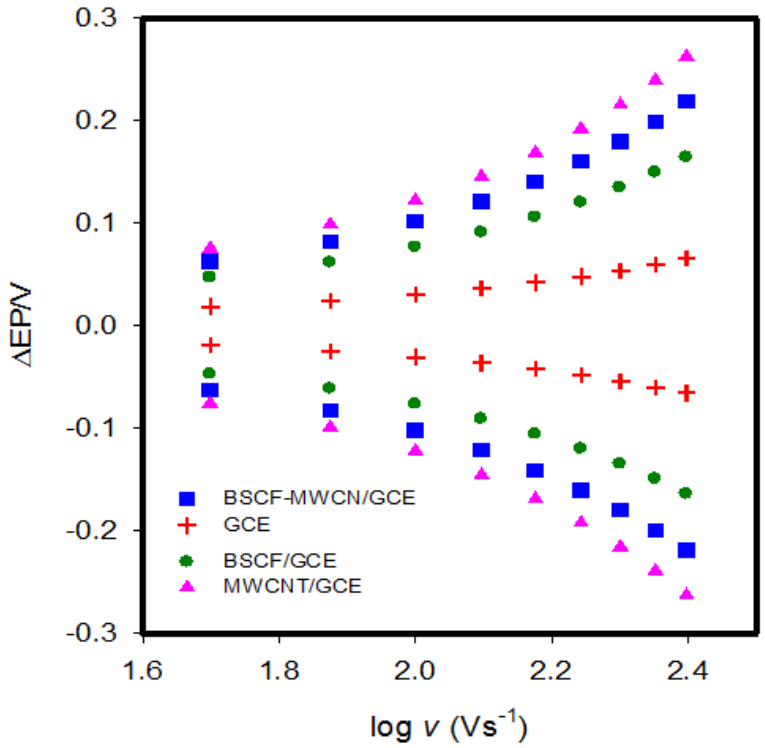

Figure 4. Plots of the peak potentials versus the logarithms of the scan rates

Table 2. Charge transfer coefficient, α and electron transfer rate constant, k_s of the electrodes in 5 mM $[Fe(CN)_6]^{4-/3-}$ and 0.1 M KCl

Electrodes	charge transfer coefficient, α	electron transfer rate constant, k_s/s^{-1}
GCE	0.43	4.42
MWCNT/GCE	0.46	3.85
BSCF/GCE	0.37	4.98
BSCF-MWCNT/GCE	0.41	4.74

3.3. Electrochemical Impedance Spectroscopy

Electrochemical impedance spectroscopy (EIS) of the electrodes were performed in a 5.0 mmol L^{-1} $K_3Fe(CN)_6$ and 0.1 mol L^{-1} KCl and frequency range of 100 kHz to 100 mHz. It shows that there is interfacial electron transfer resistance in the Nyquist plot of BSCF/GCE but this does not exist in bare GCE, MWCNT/GCE and BSCF-MWCNT/GCE (Figure 5a). The electron exchanged between the redox probe and the smooth surface of GC might be blocked by the presence of BSCF molecules on the GC surface. In Randles equivalent circuit (Figure 5b); the MWCNT/GCE, BSCF/CGE and BSCF-MWCNT/CGE composites electrodes are fitted with the model. The double-layer capacitance is replaced with a constant phase element (CPE) in the circuit to obtain a satisfactory fitting of Nyquist diagrams. The coating of MWCNT on the BSCF has decreased the resistance by 140 folds implying

that the BSCF-MWCNT is an excellent electric conducting material and has accelerated the electron transfer. The Bode plot also demonstrate that the BSCF/GCE is a good capacitor at higher frequency but pure resistor at lower frequency range (Figure 5c). Larger relaxation (−80° at 0.1 Hz) with more refined and narrower distribution peak is detected at BSCF-MWCNT/GCE, indicates the electrode coating has enhance the rate of electron transfer. In Table 3, a remarkable increase in apparent standard rate constant, k_{app} values is obtained once MWCNT becomes a component of the composite on the GCE. Incidentally, this is in good agreement with the CV result.

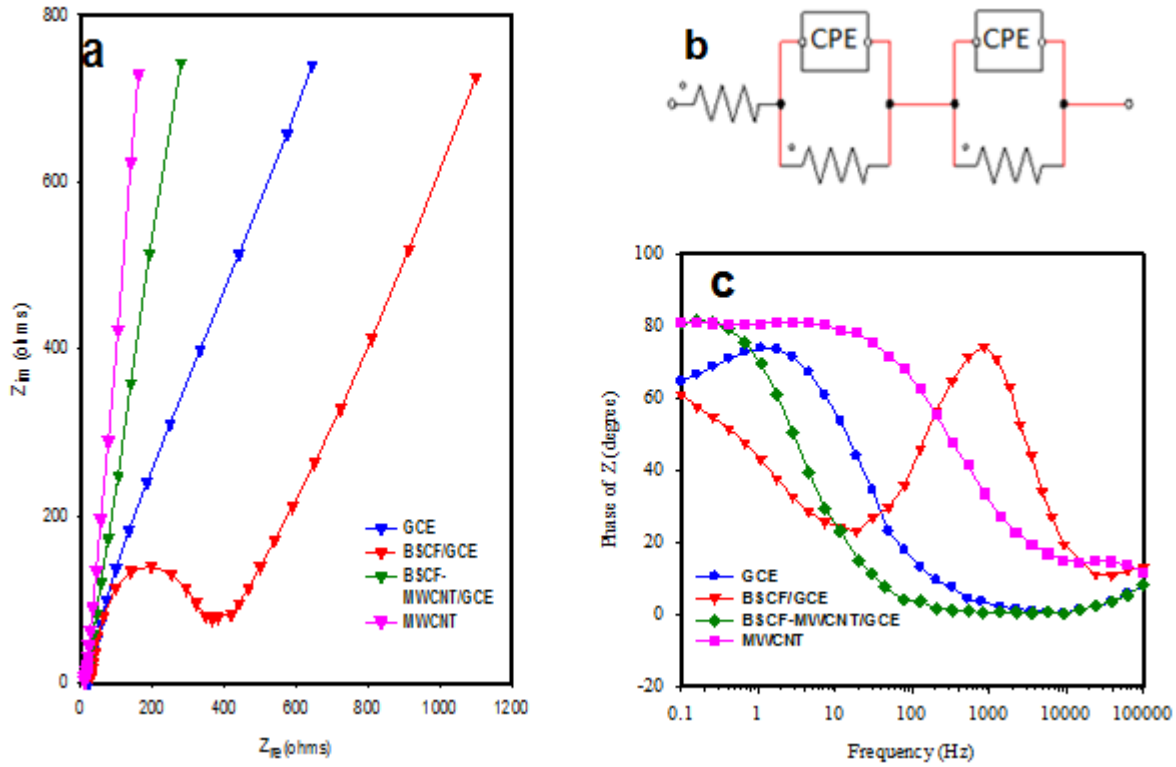

Figure 5. (a) Nyquist plot (b) Randle's equivalent electrical circuit and (c) Bode plot of 5 mM $[Fe(CN)6]^{4-/3-}$ in 0.1 M KCl at bare GCE, BSCF/GCE, MWCNT/GCE and BSCFMWCNT/GCE

Table 3. Various parameters of BSCF and BSCF-MWCNT

Electrodes	$R_s/\Omega cm^2$	$CPE/\Omega^{-1}cm^{-1}S_n$	$R_{ct}/\Omega cm^2$	k_{app}/cms^{-1}
GCE	32.12	0.000603	24.5	9.46×10^{-7}
MWCNT/GCE	10.1	0.000998	5.27	2.21×10^{-4}
BSCF/GCE	10.7	0.001410	313.0	3.13×10^{-7}
BSCF-MWCNT/GCE	10.3	0.000722	2.25	2.74×10^{-4}

3.4. Electrocatalytic oxygen reduction by cyclic voltammetry

The ORR process consist of a number of individual reactions. Generally, two ORR processes are usually examined for its electrocatalytic activity as each process consist of several discrete steps. The first process is direct four-electron pathway producing water and the second process is two-electron pathway which produce hydrogen peroxide and water. To obtain a successful ORR, a catalyst must possess the ability to reduce oxygen molecules to water through the four-electron route. Incomplete reduction of oxygen to hydrogen peroxide not only leads to lower energy conversion efficiency, but also produces reactive intermediate that can further be converted to harmful free radical species [39]. From Figure 6 it can be seen that all electrodes show O_2 reduction activity with MWCNT/GCE electrodes undergoes reduction process at most positive cathodic peak potential, E_{pc} at -0.1 V. Two irreversible peak current observed at bare GCE and modified BSCF/GCE. The cathodic peak current, I_{pc} of BSCF/GCE has increased at two folds attributable to larger specific surface area caused by high surface-to-volume ratio. The I_{pc} at the low overpotential is attributed to 2 electron reduction to H_2O_2 and at more negative potentials the peroxide intermediate is further reduced. Once MWCNT is included in only a single cathodic peak potential, E_{pc}, which has shifted positively is observed. This enhanced catalytic activity could be due to stabilization of the complex by π–π stacking on nanotubes and the participation of nanotubes in the electron transfer process. The I_{pc} of the modified BSCF-MWCNT/GCE is 10 folds of that of BSCF/GCE and 2 folds of that MWCNT/GCE attributing to higher surface-to-volume ratio of nanosized MWCNT. The ORR suggests a direct 4 electron reduction of oxygen to water.

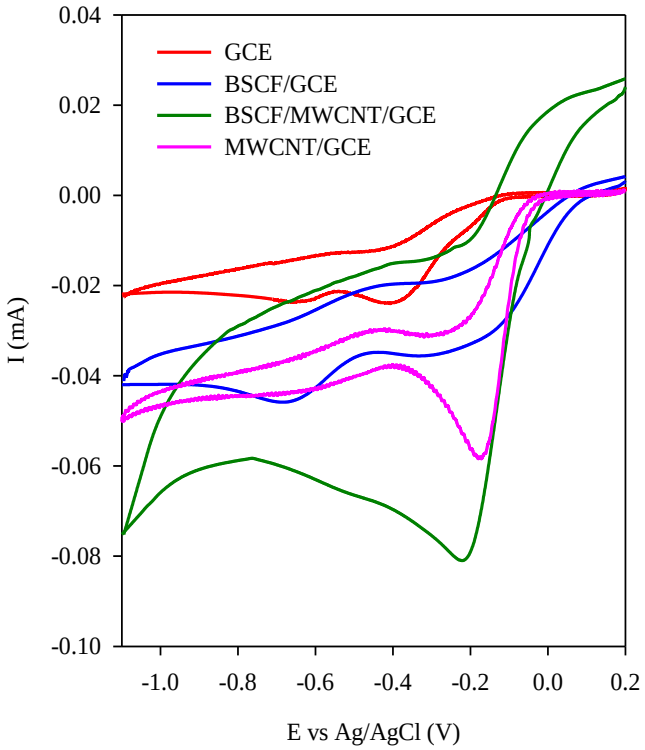

Figure 6. CV of ORR in 0.1 M KOH at 25 °C of GCE, BSCF/GCE, MWCNT/GCE and BSCFMWCNT/GCE .

3.6. Hydrodynamic studies

Rotating disk electrodes (RDE) studies was implied to obtain a steady state by keeping the electrodes at a stationary potential. RDE studies was used to support the investigation of the electrocatalytic process of ORR at the modified electrodes by cyclic voltammetry since mass transport effects of dissolved gases in liquid electrolytes can affect the rate-controlled process. Hence, the rates of mass transfer at the surface of a RDE would be much greater than those of charge transfer [9]. Accordingly, the influence of the effect of mass transfer to the electron transfer kinetics will be lesser. Therefore, the ORR was investigated with the rotating modified electrodes to obtain the kinetic parameters.

Figure 7 compares the RDE results obtained with BSCF/GCE, MWCNT/GCE and BSCFMWCNT/GCE at a single rotation rate (N = 100 rpm). It shows large differences in ORR activity of the electrodes studied. As shown, MWCNT/GCE gives the lowest onset potential ca. -0.2 V indicating its excellent electrocatalytic activity towards oxygen. However, highest current densities for ORR at a given rotation rate is observed at BSCF-MWCNT/GCE which attributes to improved kinetics due to a higher number of electrons involved in O_2 reduction. The lower current density and more negative onset potential of BSCF/GCE indicates a considerably lower activity for ORR. Therefore, BSCF-MWCNT/GCE supports more facile O_2 reduction and is chosen for the further studies.

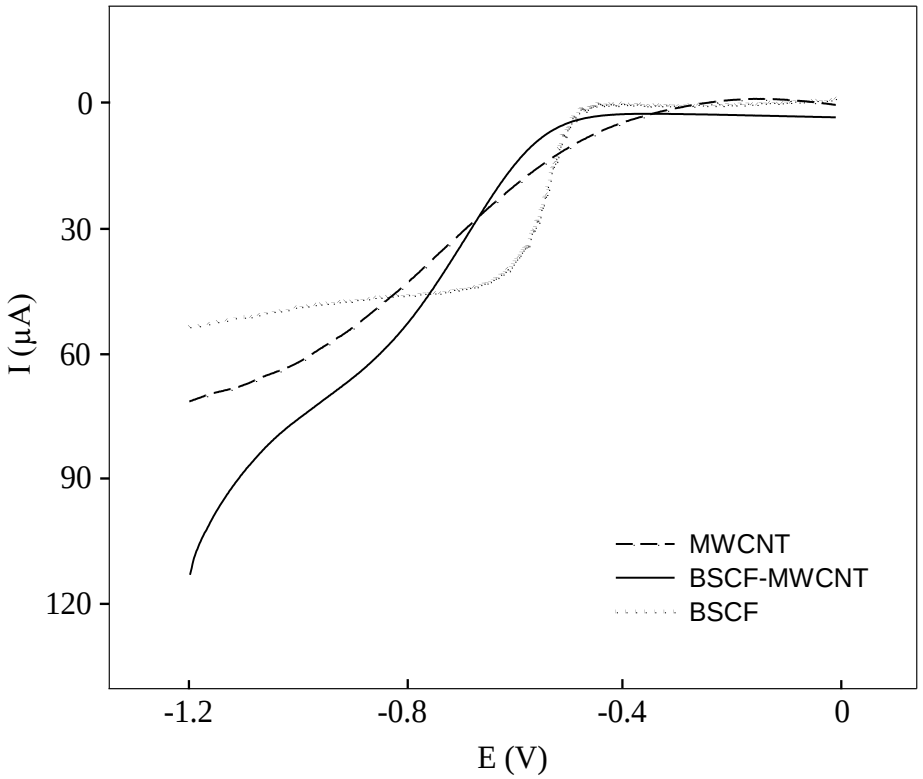

Figure 7. RDE of MWCNT, BSCF-MWCNT and BSCF on rotating glassy carbon electrode at 100 rpm in 0.1 M KOH

Figure 8 shows a set of current–potential curves recorded in an O_2-saturated 0.1 M KOH at various angular velocities (ω), with a rotating disk GCE on BSCF-MWCNT. There is no electrocatalytic activity occurs with the absence of O_2. The onset potential for O_2 reduction for BSCF-MWCNT/GCE is about −0.4 V and were gradually shifted to more positive potential with increase of the rotation rate indicating its high catalytic activity towards oxygen reduction. Well-defined limiting current plateau is observed at different rotation rates as reduction current gradually increases to a diffusion-limited value. The plateau current, also known as limiting current I_l is associated to rotation rate and can be obtained by Levich equation.

$$I_l = 0.62nFAD_{O_2}^{1/2}\nu^{-1/6}C_{O2}\omega^{1/2} \quad (6)$$

where n is the number of electrons transferred, CO_2 is the oxygen concentration in the bulk (1.29×10^{-6} mol cm^{-3}), DO_2 is the diffusion coefficient of oxygen (1.73×10^{-5} cm^2 s^{-1}) and ν is the kinematic viscosity of the solution (0.01 cm^2 s^{-1}), N is frequency in revolution per second, ω (= 2πN) is angular velocity and other symbols have their usual significance. Figure 9 represents the plots of I_l versus $\omega^{1/2}$ and linear plots obtained indicates the Levich relationship of RDE. The Levich plot, derived from the limiting current measured at a potential of -0.8 V is close to the theoretically calculated line for a four-electron process (n=4). However, a slight negative deviation at higher ω values is observed due the result of catalytic reduction in which a current-limiting chemical step precedes the transfer of electron.

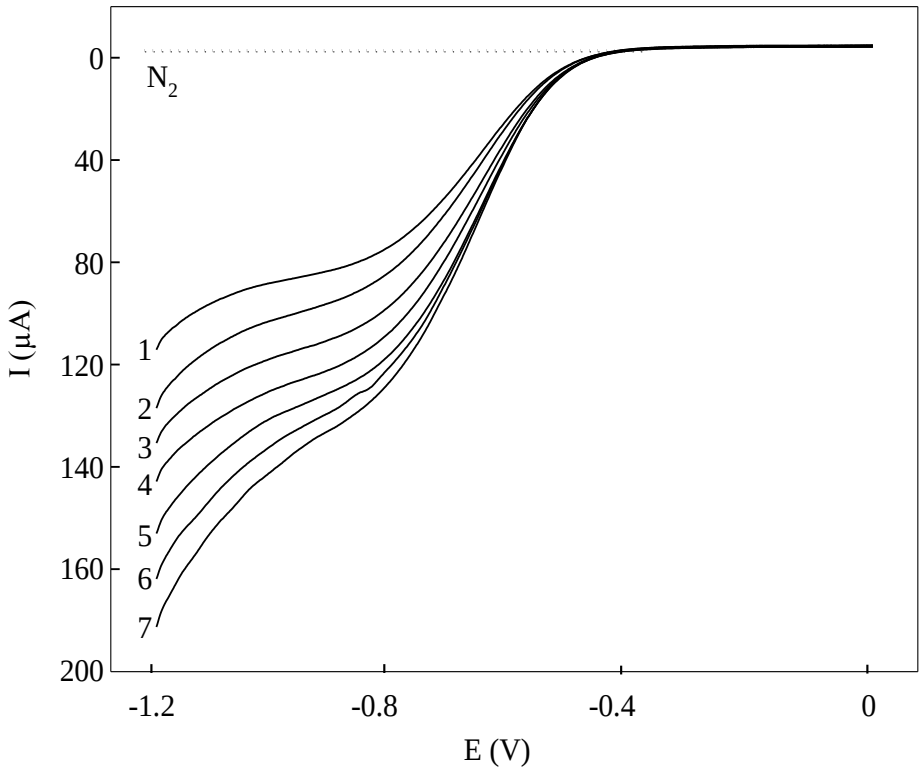

Figure 8. Rotating disk voltammograms for O_2 reduction on BSCF-MWCNT/GCE electrode in O2 saturated 0.1 M KOH. Speed of rotation (1) 100, (2) 200, (3) 400, (4) 800, (5) 1200, (6), 1600, (7) 2000 rpm.

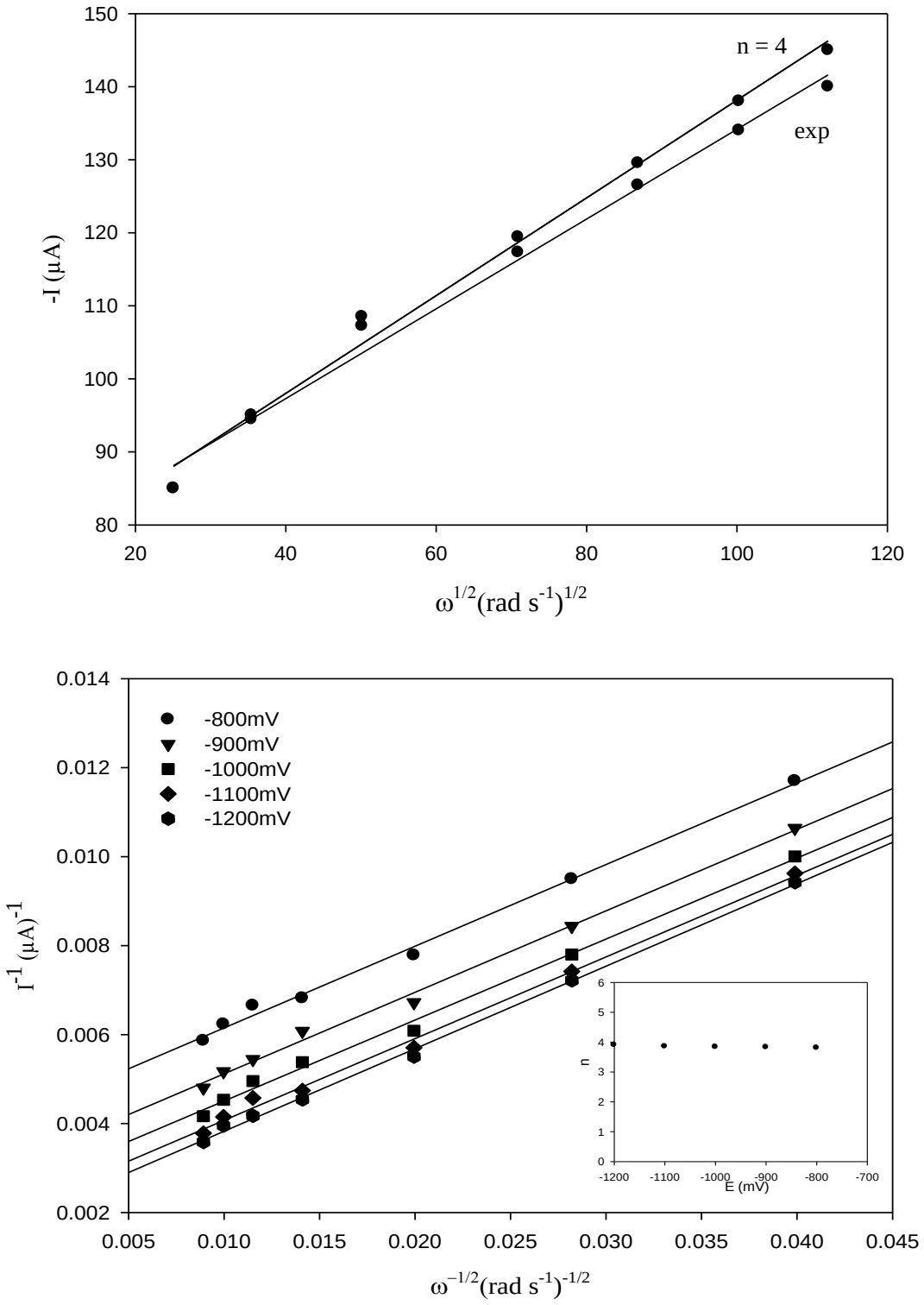

Figure 10. Levich plot of limiting current at -0.8 V and theoritical Levich plot for four (n=4) electron reduction of O_2 (b) Koutecky- Levich plots for O_2 reduction in 0.1 M KOH at various potential. Inset: Calculated potential dependance of n.

For potentials more negative than -0.8 V, these results were analyzed using the Koutecky Levich (K.L.) equation:

$$\frac{1}{j} = \frac{1}{jk} + \frac{1}{jd} = -\frac{1}{nFkC_{O_2}} - \frac{1}{0.62nFAD_{O_2}{}^{2/3}v^{-1/6}C_{O_2}\omega^{1/2}} \quad (7)$$

where j is the current density, j_k and j_d are the kinetic and diffusion-limited current densities, respectively, and k is the overall rate constant for O_2 reduction. The corresponding plots are shown in Figure 10. The Koutecky–Levich plots are well-aligned and show a linear relationship at different potentials, indicating first order kinetics for molecular oxygen reduction. Parallel plots with decreasing intercepts indicate that the reaction becomes mass transfer controlled at more negative potentials. The value of n was calculated from the slopes of the K.L. plots and reaches a value close to 4 electrons at sufficiently negative potentials (e.g.,-1.2 V). The result confirms that BSCF-MWCNT/GCE undergoes four-electron ORR (see Eq. 1). The non-zero value of the intercept implies that the ORR is under the mixed kinetic-diffusion control in a wide region of potentials. The values of rate constants (k) are calculated as $(9.32 \pm 1.5) \times 10^{-5}$ cm s^{-1} .

4. CONCLUSION

MWCNT/GCE, BSCF/GCE and BSCF-MWCNT/GCE have been optimized for ORR. The study shows that MWCNT is capable to form a uniform distribution and compatible with the BSCF. MWCNT acts as a modifier and has increased the electroactive surface area of the electrodes. The modified electrodes have exhibited excellent electrocatalytic activity towards ORR. The presence of MWCNT is proven to have enhanced the electrocatalysis.

ACKNOWLEDGMENT
This work was supported by the Ministry of Higher Education (MHE) Fundamental Research Grant Scheme (FRGS) 203/PKIMIA/6711263 and Research Acculturation Grant Scheme (RAGS) RAGS/1/2015/ST0/UMT/03/2.

References

1. K. Gong, F. Du, Z. Xia, M. Durstock and L. Dai, *Science*, 323 (2009) 760.
2. J. Suntivich, H.A. Gasteiger, N. Yabuuchi, H. Nakanishi, J.B. Goodenough and Y. Shao-Horn, *Nature Chem .*, 3 (2011) 546-550.
3. A. Damjanovic, M. Genshaw and J.M. Bockris, *J. Electrochem. Soc.*, 114 (1967) 466-472.
4. M. Lai and A. Bergel, *J. Electroanal. Chem.*, 494 (2000) 30-40.
5. L. Nei and R.G. Compton, *Sensor Actuat B-Chem.*, 30 (1996) 83-87.
6. I. Roche, E. Chaînet, M. Chatenet and J. Vondrák,, *J. Phys. Chem. C.*, 111 (2007) 14341443.
7. D. Geng, Y. Chen, Y. Chen, Y. Li, R. Li, X. Sun, S. Ye and S. Knights, *Energy Environ. Sci.*, 4 (2011) 760-764.

8. J.M. Ziegelbauer, T.S. Olson, S. Pylypenko, F. Alamgir, C. Jaye, P. Atanassov and S. Mukerjee, *J. Phys. Chem. C*, 112 (2008) 8839-8849.
9. P. Manisankar , A. Gomathi and D. Velayutham, *J. Solid State Electrochem*., 9(2005) 601–608.
10. Y. Lin, X. Cui and X. Ye, *Electrochem. Commun.*, 7 (2005) 267-274.
11. J. Zhai, M. Huang and S. Dong, *Electroanal.*, 19 (2007) 506-509.
12. M. Calegaro, F. Lima and E. Ticianelli, *J. Power Sources*, 158 (2006) 735739.
13. S. Tsujimura, Y. Kamitaka and K. Kano, *Fuel Cells*, 7 (2007) 463-469.
14. A. Venugopal, J. Aluha, D. Mogano and M.S. Scurrell, *Appl Catal A Gen.*, 245 (2003) 149-158.
15. J. Zagal, M. Paez and A. Tanaka, *J. Electroanal. Chem.*, 339 (1992) 13-30.
16. Z. Shi and J. Zhang, *J. Phys. Chem. C*, 111 (2007) 7084-7090.
17. J. Suntivich, K.J. May, H.A. Gasteiger, J.B. Goodenough and Y. Shao-Horn, *Science*, 334 (2011) 1383-1385.
18. D. Meadowcroft, *Nature*, 226 (1970) 847 - 848.
19. T. Hyodo, M. Hayashi, N. Miura and N. Yamazoe, *J. Electrochem. Soc.*, 143 (1996) L266-L267.
20. T. Hyodo, N. Miura and N. Yamazoe, *Gas Diffusion-Type Oxygen Electrode Using Perovskite-Type Oxides for Metal-Air Batteries, in: Materials Research Society Symposium Proceedings* Cambridge Univ Press, United Kingdom (1995)
21. M. Doyle, G. Rajendran, W. Vielstich, H.A. Gasteiger and A. Lamm, *Handbook of Fuel Cell Fundamentals, Technology, and Applications*, John Wiley, United Kingdom (2003)
22. M. Arnold, W. Haihui and A. Feldhoff, *J. Membrane Sci.*, 293 (2007) 44-52.
23. P. Zeng, Z. Chen, W. Zhou, H. Gu, Z. Shao and S. Liu, *J. Membrane Sci*, 291 (2007) 148156.
24. W. Zhou, Z. Shao, R. Ran, W. Jin and N. Xu, *Chem. Commun.*, (2008) 5791-5793.
25. S. Li, Z. Lu, B. Wei, X. Huang, J. Miao, Z. Liu and W. Su, *J. Alloy Compd.*, 448 (2008) 116–121.
26. T. Schmidt, H. Gasteiger, G. Stäb, P. Urban, D. Kolb and R. Behm, *J. Electrochem. Soc.*, 145 (1998) 2354-2358.
27. M.A. Harmer, W.E. Farneth and Q. Sun, *J. Am. Chem. Soc.*, 118 (1996) 77087715.
28. A.L.M. Reddy, M.M. Shaijumon, S.R. Gowda and P.M. Ajayan, *Nano Lett.*, 9 (2009) 1002-1006.
29. L.-C. Qin, X. Zhao, K. Hirahara, Y. Miyamoto, Y. Ando and S. Iijima, *Nature*, 408 (2000) 50-50.
30. S. Lee, Y. Lim, E.A. Lee, H.J. Hwang and J.-W. Moon, *J. Power Sources*, 157 (2006) 848-854.
31. Y. Wei, G. Eres, V. Merkulov and D. Lowndes, *Appl. Phys. Lett.*, 78 (2001) 1394-1396.
32. S. Hofmann, R. Sharma, C. Ducati, G. Du, C. Mattevi, C. Cepek, M. Cantoro, S. Pisana, A. Parvez and F. Cervantes-Sodi, *Nano Lett.*, 7 (2007) 602-608.
33. H.-F. Cui, J.-S. Ye, X. Liu, W.-D. Zhang and F.-S. Sheu, *Nanotechnology*, 17 (2006) 2334.
34. M. Zheng, A. Jagota, M.S. Strano, A.P. Santos, P. Barone, S.G. Chou, B.A. Diner, M.S. Dresselhaus, R.S. Mclean and G.B. Onoa, *Science*, 302 (2003) 1545-1548.
35. H. Wei, S.N. Kim, M. Zhao, S.-Y. Ju, B.D. Huey, H.L. Marcus and F. Papadimitrakopoulos, *Chem. Mat.*, 20 (2008) 2793-2801.
36. S. Wang, Q. Zhang, R. Wang and S. Yoon, *Biochem. Biophys. Res. Commun.*, 311 (2003) 572576.
37. W. Zhou, R. Ran, Z.P. Shao, H.X. Gu, W.Q. Jin and N.P. Xu, *J. Power Sources*, 174 (2007) 237-245.
38. F. Yusoff, M. Norita, A. Aziz and S. Ab Ghani, *Int. J. Electrochem. Sci.*, 8 (2013) 10672- 1068.
39. B. Wang, *J. Power Sources*, 152(2005)1-15.